Electrochemistry Communications 115 (2020) 106736

Contents lists available at ScienceDirect

Electrochemistry Communications

journal homepage: www.elsevier.com/locate/elecom

Investigation of the effects of Pt/Pd composition and PVP content on the activity of Pt/Pd core-shell catalysts

Katsumasa Matsumoto[a,b], Masataka Hiyoshi[c], Takashi Iijima[c], Hidenori Noguchi[a,d,*], Kohei Uosaki[d,*]

[a] Graduate School of Chemical Sciences and Engineering, Hokkaido University, Sapporo 060-8628, Japan
[b] Nippon Steel Corporation, Technical Research & Development Bureau, 1-8 Fuso-Cho, Amagasaki 660-0891, Japan
[c] Nippon Steel Corporation, Technical Research & Development Bureau, 20-1 Shintomi, Futtu 293-8511, Japan
[d] Center for Green Research on Energy and Environmental Materials, National Institute for Materials Science, 1-1 Namiki, Tsukuba 305-0044, Japan

ARTICLE INFO

Keywords:
Polymer electrolyte fuel cell
Core–shell catalyst
MEA
SEIRAS

ABSTRACT

Among the various fuel cell electrocatalysts studied for the cathodic oxygen reduction reaction and anodic fuel oxidation reaction, platinum-based materials have attracted much attention over the past decade because of their high activity for both reactions. However, Pt-based catalysts suffer from several problems, such as their high cost, low abundance, and low long-term stability. Bimetallic Pt-based nanostructures with a core–shell structure have been considered as candidate cathode catalysts for polymer electrolyte fuel cells. In this study, a Pt/Pd/C catalyst was successfully synthesized by the hydrogen-sacrificial protection method to improve the performance of a membrane electrode assembly. Furthermore, on the basis of electrochemical spectroscopic findings, it was shown that control of the surface structure is an effective strategy to improve the cell performance of the Pt/Pd/C catalyst.

1. Introduction

Polymer electrolyte fuel cells (PEFCs) have found considerable practical use in fuel cell vehicles (FCVs). To promote the wider uptake of FCVs, it is important to reduce the use of expensive Pt-based catalysts. The cell performance of FCVs is especially dependent on control of the oxygen reduction reaction (ORR) on cathodic Pt catalysts, because the ORR is kinetically slower than the anodic hydrogen oxidation reaction. To minimize Pt usage without loss of ORR activity, many approaches to catalyst development have been reported. One promising approach is the deposition of thin Pt overlayers on non-noble or noble metal substrates to make a Pt skin, resulting in core–shell structures which change the electronic structure of the catalyst to enhance the ORR activity, and hence reduce the usage of Pt [1–6].

One method for fabricating a core–shell structure is to coat several atomic layers of Pt onto particles of another metal. However, it is essential for the other metal to have almost the same crystal structure as Pt (face-centered cubic lattice, similar atomic radius) for epitaxial growth to occur. Additionally, it is necessary to select a metal species that can be phase-separated from Pt. To meet these requirements, core–shell nanoparticle catalysts with a Pd core and a Pt shell have been investigated. For example, J. Zang et al. studied the ORR on a Pt shell deposited on Pd nanoparticles, which was formed by the galvanic displacement of an underpotentially deposited Cu monolayer by Pt atoms on the Pd surface [3]. Meanwhile, Wang et al. studied the ORR on a Pt shell deposited on Pd by a colloidal method using hydrogen as a reducing agent [7,8].

However, these previous studies were only concerned with electrochemical evaluation, and did not report the cell performance of these materials as cathodes in a membrane electrode assembly (MEA). When a colloidal agent (surfactant) adheres to nanoparticles, the cell performance may be impaired because the catalyst surface is effectively polluted by the surfactant. The removal of the surfactant to preserve cell performance has been reported by several groups and showed that the heat-treated catalysts show high ORR activity [9–11]. However, there is no detailed information about the structural changes in Pd core/Pt shell catalysts induced by heat treatment.

In this study, we report the cell performance of an MEA based on a Pt/Pd/C catalyst formed by the hydrogen sacrificial protection method, and discuss the effect of catalyst surface conditions on the performance.

This method can be used to easily control bi- or multi-metallic materials using the reduction reaction induced by hydrogen absorbing

* Corresponding authors at: Center for Green Research on Energy and Environmental Materials, National Institute for Materials Science, 1-1 Namiki, Tsukuba 305-0044, Japan (H. Noguchi).
E-mail addresses: NOGUCHI.Hidenori@nims.go.jp (H. Noguchi), UOSAKI.Kohei@nims.go.jp (K. Uosaki).

https://doi.org/10.1016/j.elecom.2020.106736
Received 19 February 2020; Received in revised form 16 April 2020; Accepted 22 April 2020
Available online 29 April 2020

on the substrate (core nanoparticles). The hydrogen sacrificial protection method does not involve any contaminating mediators, such as Cu. Furthermore, this procedure is effective for industry because precise potential control is not required [8].

2. Material and methods

2.1. Chemicals

$PdCl_2$ (Kojima Chemicals) and K_2PtCl_4 (Kojima Chemicals) were used as Pd and Pt precursors, respectively, for the colloidal catalysts. Carbon powder (Ketjen black: EC600JD, Lion Specialty Chemicals) was used as a support for the colloidal catalysts. Polyvinylpyrrolidone (PVP: MW = 10,000, Tokyo Kasei Kogyo) was used as a colloid-protective agent and ethylene glycol (Kanto Chemical) was used as a reducing agent for the Pt and Pd nanoparticles.

2.2. Preparation

Pd–core colloidal solutions were prepared in a flask (equipped with a dropping funnel) containing a mixture of 1.0 M $PdCl_2$ aqueous solution, ethylene glycol, and PVP. First, the solution was stirred for 30 min at room temperature while introducing Ar gas with a flow rate of 50 mL/min. Then the temperature was increased to 160 °C and held for 180 min under Ar gas with a flow rate of 50 mL/min to obtain the Pd core. After cooling the Pd solution to room temperature, H_2 gas was introduced into the solution for 90 min to adsorb H_2 onto the Pd core. After that, Ar gas was introduced into the solution for 30 min to degas the remaining H_2 in the solution. To prepare the Pt shell structure on the Pd core colloidal solution, 4 mM K_2PtCl_4 aqueous solution was added to the Pd core solution under Ar gas flow for 10 h. Ketjen black powder was added to the Pd core/Pt shell (Pt/Pd) colloidal solution at 90 °C for 1 h to prepare Pt/Pd nanoparticles on the carbon support [12]. After cooling the mixed solution of Pt/Pd colloid and carbon to room temperature, the solution was suction-filtered three times using a 0.2 μm pore membrane filter and distilled water. Finally, a black powder was obtained and evacuated at 90 °C for 300 min, and was subsequently used as a catalyst comprising a Pd core/Pt shell on a carbon support (Pt/Pd/C).

To investigate their catalytic properties, the Pt/Pd/C catalysts were further heat-treated at either 200 or 300 °C under either air or H_2. The Pt/Pd/C catalysts obtained using different heat and gas options are denoted as (Atmosphere)-(Temperature)-(Time)-Pt/Pd/C and the treatments under different conditions are summarized in Table 1. A Pt-only catalyst (Pt/C) and a Pd-only catalyst (Pd/C) were also synthesized by the colloidal method as described above.

2.3. Characterization

2.3.1. TEM measurement

The catalyst structure and composition were determined by a transmission electron microscope (TEM: JEM-ARM200F, JEOL) equipped with an energy-dispersive X-ray spectroscopy (EDS: JED-2300T, JEOL) system. High-Angle Annular Dark-Field Scanning Transmission Electron Microscopy (HAADF-STEM) was performed at an accelerating voltage of 200 kV.

2.3.2. Thermogravimetric analysis

Thermogravimetric/differential thermogravimetric analysis (TG-DTA; Thermo plus, Rigaku) was performed at 10 °C/min under air flowing at a rate of 100 mL/min.

2.4. Electrochemical FTIR measurement

To characterize the surface properties of the catalyst, an FTIR spectrometer (FT/IR6200, JASCO) equipped with a

Table 1
Catalyst property of heat treated Pt/Pd/C, Pt/Pd/C, Pt/C, and Pd/C.

Samples	Atmosphere	Temperature (°C)	Time (min.)	Pt content (wt%)	Pd content (wt%)	Particle size※(nm)	PVP residual (wt%)	CO bridge (Pd)/CO on top site (Pt)※※	Estimated Surface components
Air-300–20-Pt/Pd/C	Air	300	20	24 ± 1.4	13 ± 0.8	3.7 ± 0.07	2.2 ± 0.9	1.68	Pt, Pd
Air-300-30-Pt/Pd/C	Air	300	30	20 ± 3.4	13 ± 0.3	3.8 ± 0.43	1.0 ± 0.7	1.98	Pt, Pd
H2-200-20-Pt/Pd/C	H_2	200	20	21 ± 1.2	11 ± 0.3	3.7 ± 0.13	3.2 ± 1.1	0.17	Pt, Pd
H2-300-20-Pt/Pd/C	H_2	300	20	22 ± 0.3	12 ± 0.6	4.2 ± 0.02	2.1 ± 1.2	2.29	Pt, Pd
Pt/Pd/C	—	—	—	20 ± 0.4	11 ± 0.1	3.0 ± 0.02	5.0 ± 1.3	0.00	Pt,
Pt/C	—	—	—	20 ± 0.2	0	2.5 ± 0.13	5.2 ± 0.3	0.00	Pt,
Pd/C	—	—	—	0	14 ± 0.1	2.1 ± 0.30	1.9 ± 0.7	—	Pd

※The average crystallite size was calculated by using the Scherrer's equation from X-Ray Diffraction patterns at (2 2 0).
※※The integrated peak area ratio of the CO bridge site/CO on top site by using SEIRAS.

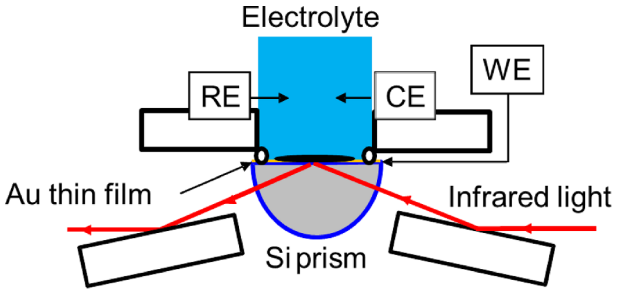

Fig. 1. Schematic configuration for electrochemical SEIRAS measurement.

spectroelectrochemical cell was used, as shown in Fig. 1. A thin film of Au was electrolessly deposited on the reflecting plane of an attenuated total reflection semicylindrical Si prism (12.5 mm radius and 25 mm length, Pier Optics) for surface-enhanced infrared absorption spectroscopy (SEIRAS) [13].

The catalysts on the Au film were used as the working electrode. Ag/AgCl (saturated NaCl) and Pt wire were used as the reference and counter electrodes, respectively. Electrochemical FTIR measurements were carried out in a 0.05 M H_2SO_4 (Kanto Chemicals) electrolyte solution.

A methanol (Kanto Chemical) solution was added to 20 mL of the H_2SO_4 electrolyte solution in the spectroelectrochemical cell to adjust the electrolyte concentration to 1.0 M at 0.1 V. The SEIRAS measurements were carried out under a flow of N_2 gas into the electrolyte solution. Background spectra were measured in H_2SO_4 electrolyte solution at each potential to obtain the absorbance spectra in the presence of added methanol in order to observe the surface-adsorbed CO on the catalyst. The reference spectrum at 1.0 V was used to plot changes in the absorbance spectra.

2.5. Fuel cell performance test

The structure of the MEAs was as follows: anode: Pt/C; cathode: Pt/Pd/C, heat-treated Pt/Pd/C, or Pt/C; and membrane: perfluorosulfonic acid membrane (Nafion NR212). The Pt loading of the catalysts used for the cathode was 0.10 mg/cm^2 for Pt/Pd/C, heat-treated Pt/Pd/C, and Pt/C. We also tried a different Pt loading of 0.18 mg/cm^2 of Pt/C on the cathode to demonstrate the effect of the Pd core shell catalyst. The Pt loading of the catalyst used for the anode was 0.10 mg/cm^2.

The MEAs were prepared by a spraying method [14]. The catalyst ink was sprayed onto a PTFE membrane through a nozzle, and dried to obtain a catalyst layer. The resulting catalyst layer was sandwiched with Nafion and hot pressed at 135 °C for 5 min to obtain a MEA. The geometric active area of the prepared MEA was 13 cm^2 (36 × 36 mm) and the MEA was assembled into a single fuel cell using a gas diffusion layer (SGL35BC, SGL). The performance of the fuel cell was tested using a fuel cell test system (PEMTest890, Scribner Associates) under conditions of high humidity [14]. The cell voltage was obtained by scanning the current to evaluate the activation overvoltage of the catalyst particles.

3. Results and discussion

Fig. 2 shows the HAADF-STEM images and EDS line profiles for the various samples. In the case of the Pt/Pd/C catalyst, the edge of the sample was rich in Pt, while the core was rich in Pd. From this result, we can conclude that the core–shell structure of the Pt/Pd/C catalyst had been successfully constructed.

With a longer heat treatment time under air (Air-300-30-Pt/Pd/C), the Pt shell was less sharply separated from the Pd core than with shorter heat treatment (Air-300-20-Pt/Pd/C). Heat treatment under a H_2 atmosphere (H2-300-20-Pt/Pd/C) also promoted the mixing of the Pt shell and the Pd core relative to the sample heat-treated under air (Air-300-20-Pt/Pd/C). This result implies that the aggregation of nanoparticles on the carbon supports was accelerated by heat treatment under hydrogen.

Furthermore, under H_2, the higher temperature heat treatment (H2-300-20-Pt/Pd/C) promoted complete mixing of the Pt shell with the Pd core and yielded a larger particle size than the lower temperature heat treatment (H2-200-20-Pt/Pd/C). Atomic diffusion between Pt and Pd is evidently easier at a high temperature. It is well known that in the Pt–Pd binary system, phase separation will occur at an elemental composition ratio of Pt: 50 at%, Pd: 50 at% [15]. However, the melting point is lower for nanoparticles than in the bulk [16]. Thus, it can be assumed that Pt and Pd mixed easily, even below 300 °C.

Fig. 3 shows the SEIRAS spectra of Pt/C, Pd/C, Pt/Pd/C, and heat treated Pt/Pd/C catalysts. The Pt/C catalyst showed a SEIRAS peak around 2010 cm^{-1} while for the Pd/C catalyst the peak appeared around 1850 cm^{-1}. According to previous FTIR experiments on methanol oxidation at Pt and Pd electrodes, these peaks can be assigned to CO stretching vibrations on Pt on-top sites and Pd bridge sites, respectively [17]. In the case of the Pt/Pd/C catalyst, only one peak was observed, at 2010 cm^{-1}. This suggests that the CO was adsorbed only on the Pt surface of the Pt/Pd/C catalyst. Thus, we can conclude that the Pt/Pd/C catalyst prepared by the sacrificial hydrogen method has a core–shell structure. After heat treatment (heat-treated Pt/Pd/C), a peak at 1850 cm^{-1} was observed. This result indicates that CO was adsorbed on the Pd surface of the nanoparticles, in good agreement with the images observed by HAADF-STEM in the previous section.

With a longer heat treatment time under air (Air-300-30-Pt/Pd/C), the integrated peak area ratio of the CO bridge site and CO on-top site was increased relative to the shorter heat treatment (Air-300-20-Pt/Pd/C). Moreover, with heat treatment under H_2 atmosphere (H2-300-20-Pt/Pd/C), the integrated peak area ratio of the CO bridge site and CO on-top site increased than in the sample prepared under air atmosphere (Air-300-20-Pt/Pd/C). From these results, and the HAADF-STEM images (Fig. 2), we conclude that aggregation of nanoparticles on the carbon supports occurred in both cases, while the hydrogen atmosphere accelerated the oxidation of the carbon supports, causing the detachment of nanoparticles from the supports.

Another effect of the higher-temperature treatment (H2-300-20-Pt/Pd/C) was that the peak of the CO bridge sites was more intense than under the lower-temperature treatment (H2-200-20-Pt/Pd/C). This result suggests that diffusion of Pd atoms to the surface of the nanoparticles was promoted at high temperature.

Fig. 4 shows the TG results for the Pt/Pd/C and heat-treated Pt/Pd/C catalysts. For the Pt/Pd/C catalyst, weight loss was observed from ca. 70 °C. This weight loss can be attributed to water adsorbed on the PVP, as the decomposition temperature of PVP is much higher than 70 °C. We also examined the weight loss behavior of Pt/Pd/C (see Supporting Information). In this case, three TG-DTA peaks were observed: the first peak at 165 °C, the second at 270 °C, and the third at 400 °C. We assigned these three peaks as the decomposition of PVP on the catalyst nanoparticles, the decomposition of PVP on carbon, and the combustion of the carbon support by the catalyst, respectively.

The catalyst prepared using a longer heating time under air (Air-300-30-Pt/Pd/C) shower a smaller weight loss than that prepared with a shorter heating time (Air-300-20-Pt/Pd/C).

According to these results, as the heat energy supplied during TG-DTA increased, decomposition of PVP occurred and the bulk PVP was gradually denatured above 200 °C.

In terms of effectiveness of PVP removal, the five catalysts lie in the following order: Air-300-30-Pt/Pd/C > H2-300-20-Pt/Pd/C ≅ Air-300-20-Pt/Pd/C > H2-200-20-Pt/Pd/C ≫ Pt/Pd/C. These results show that a heat treatment at 300 °C for 30 min under an air atmosphere best facilitates the removal of PVP from the nanoparticles.

Fig. 5 shows the fuel cell performance of the Pt/Pd/C and heat-treated Pt/Pd/C and Pt/C catalysts in terms of cell voltage. The Pt/Pd/C showed better performance than Pt/C. The optimal Pt/Pd/C ((b), (c),

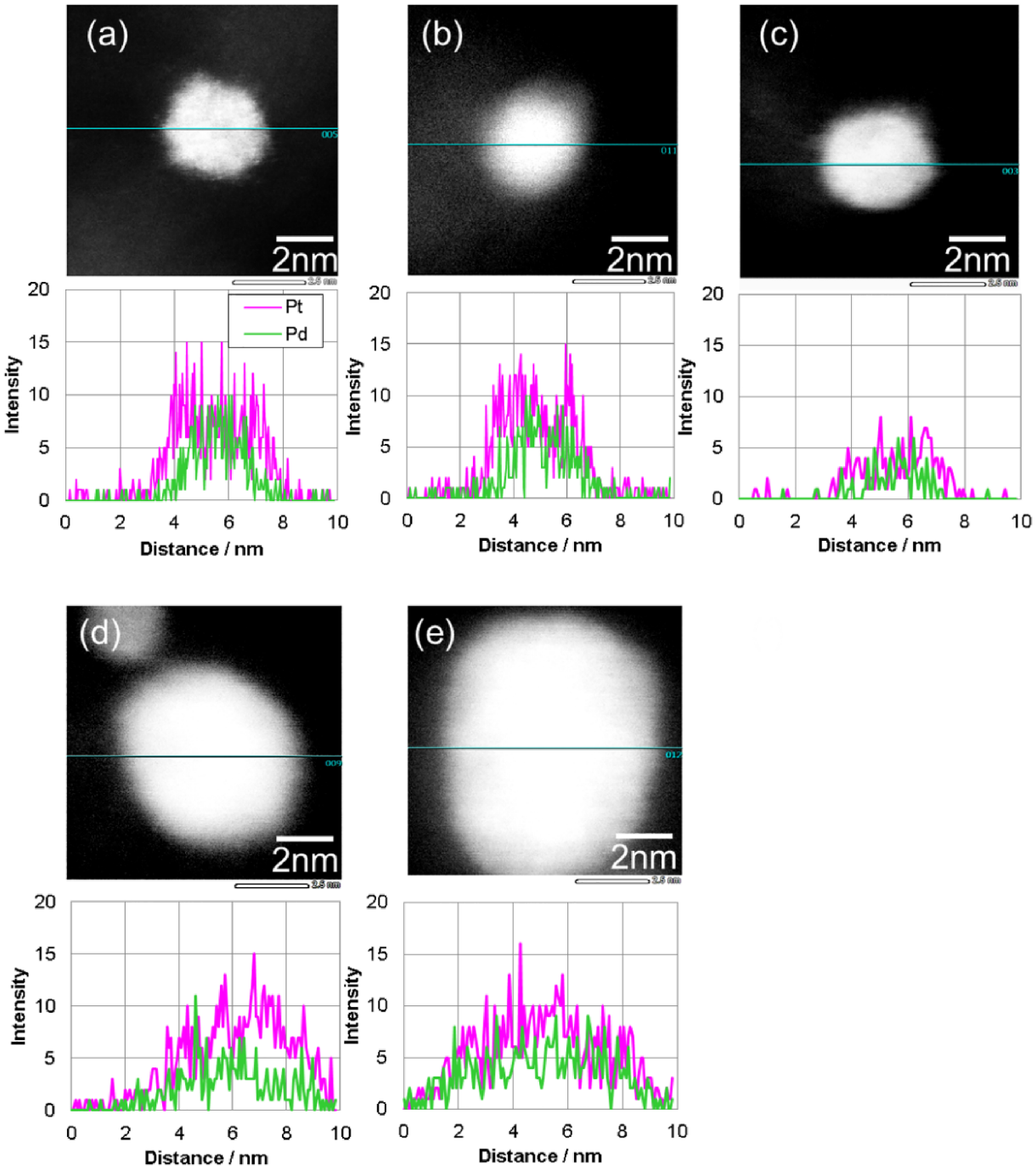

Fig. 2. HAADF-STEM images and EDS line profiles for (a) Pt/Pd/C, (b) Air-300-20-Pt/Pd/C, (c) Air-300-30-Pt/Pd/C, (d) H2-200-20-Pt/Pd/C, and (e) H2-300-20-Pt/Pd/C.

(e) the Pt loading amount was ca. 0.10 mg/cm^2) catalysts achieved a better performance than Pt/C (the Pt loading amount was ca. 0.20 mg/cm^2) despite a roughly 50% reduction in the amount of Pt used. This result indicates that preparing Pt/Pd/C catalysts by the hydrogen-sacrificial protection method is highly effective for reducing the usage of Pt in PEFCs.

The cell voltage at 200 mA/cm^2 was taken as a guide to the catalytic activity because in this potential region, the activation overpotential is dominant. The following results were observed. With a shorter heat treatment time under air (Air-300-20-Pt/Pd/C), the cell voltage was higher than with a longer heat treatment (Air-300-30-Pt/Pd/C). However, the catalyst produced by heat treatment under H_2 atmosphere (H2-300-20-Pt/Pd/C) showed almost the same voltage as that produced under air (Air-300-20-Pt/Pd/C). Under H_2 atmosphere, the higher-temperature heat treatment (H2-300-20-Pt/Pd/C) produced a catalyst with a greater cell voltage than that prepared at a lower temperature (H2-200-20-Pt/Pd/C).

According to these results, the cell performances lie in the following order:

Air-300-20-Pt/Pd/C (0.79 V) = H2-300-20-Pt/Pd/C (0.79 V) > Air-300-30-Pt/Pd/C (0.78 V) > Pt/Pd/C (0.75 V) > H2-200-20-Pt/Pd/C (0.74 V) > Pt/C (0.70 V) > Pt/C with a Pt loading of ca. 0.10 mg/cm^2.

We attributed the improved performance after heat treatment to two effects: Pt–Pd mixing and removal of PVP from the nanoparticles.

The cell performances lie in a slightly different order to that of the

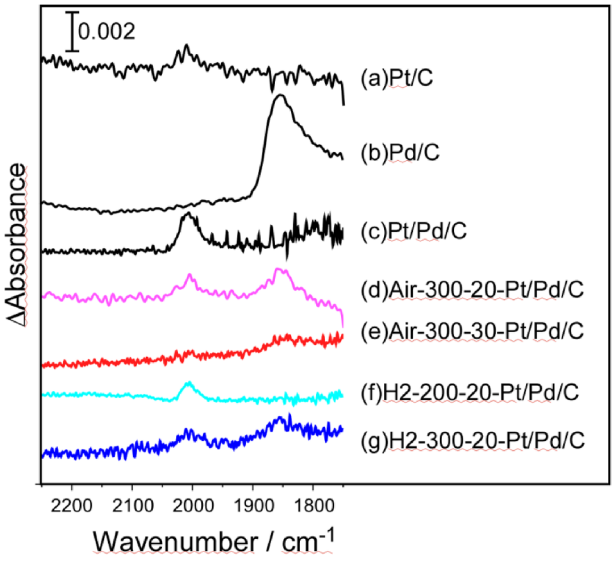

Fig. 3. SEIRAS spectra of (a) Pt /C, (b) Pd/C, (c) Pt/Pd/C, (d) Air-300-20-Pt/Pd/C, (e) Air-300-30-Pt/Pd/C, (f) H2-200-20-Pt/Pd/C, and (g) H2-300-20-Pt/Pd/C.

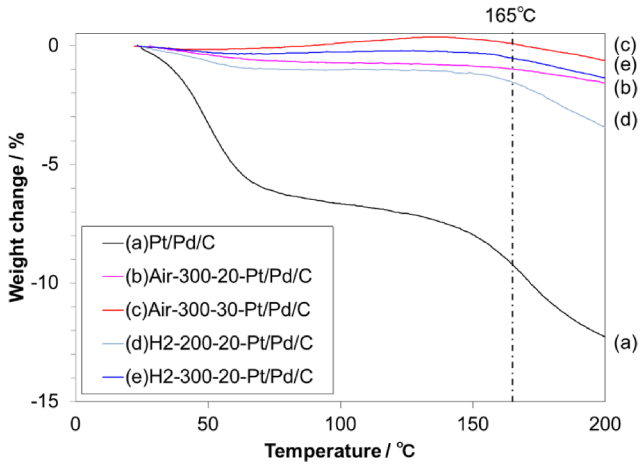

Fig. 4. TG analysis of (a) Pt/Pd/C, (b) Air-300-20-Pt/Pd/C, (c) Air-300-30-Pt/Pd/C, (d) H2-200-20-Pt/Pd/C, and (e) H2-300-20-Pt/Pd/C.

efficiency of removal of PVP from the catalyst nanoparticles mentioned above. This suggests that the fuel cell performance is affected not only by the removal of PVP but also by the surface catalyst structure of Pt and Pd. For example, even though the removal of PVP tends to improve performance, H2-200–20-Pt/Pd/C has lower performance than Pt/Pd/C despite the removal of PVP. This indicates that the surface structure of the catalyst contributes to the performance, as discussed in the analysis of the HAADF-STEM (Fig. 2) and SEIRAS (Fig. 3) results.

In terms of the catalyst structure (Table 1), the best fuel cell performance can be expected for catalysts with a mixture of Pt and Pd. This implies that it is important for the heat treatment to occur at ca. 300 °C (around the melting point of Pt and Pd nanoparticles). As described above, we surveyed the influence of time, temperature, and atmosphere on the heat treatment. It appears that temperature may be the most important factor determining the performance of this core–shell catalyst. We also confirmed that the durability of the Pt/Pd/C and heat-treated Pt/Pd/C catalysts was almost at the same level as conventional Pt/C catalysts (see Supporting Information).

Fig. 6 shows the contour plot of cell performance, with the cell voltage on the *z*-axis, the integrated peak area ratio of the CO bridge sites/CO top sites (obtained from SEIRAS measurements) on the *y*-axis, and the amount of PVP remaining on the catalyst surface (obtained from TG-DTA) on the *x*-axis. The voltages were measured at 200 mA/cm^2. The *y*-axis indicates the surface condition of the catalyst.

As the integrated peak area ratio of the CO bridge sites/CO top sites increased, the cell voltage also increased when the amount of residual PVP was low, i.e. ca. 0.5–1.5 wt% (see Fig. 6, red area). However, when the ratio increased above 2.0, the cell voltage began to fall again. This result suggests that an excess number of Pd atoms were exposed to the catalyst surface under these heat treatment conditions (see Figs. 2, 3 and Table 1). Indeed, with an increasing number of Pd atoms on the catalyst surface, the cell voltage decreased: therefore, the bare Pd/C had a lower fuel cell performance than Pt/C.

Thus, we consider that other factors also contribute to the fuel cell performance: for example, the Pt–Pt bond distance and/or amount of PVP remaining on the catalyst surface. To estimate the Pt–Pt bond distance on the catalyst surface of this core–shell structure is difficult. An earlier X-ray Absorption Fine Structure (XAFS) experiment mostly revealed information about the structure of the bulk, which was found to be partially mixed Pt–Pd bonding [18,19]. However, it is quite difficult to focus specifically on the surface structure of a core–shell catalyst. Herein, we estimated the surface properties from an electrochemical spectroscopic point of view using SEIRAS. The SEIRAS results contain information on the surface structure of the catalyst in terms of the adsorption sites of CO molecules, which vary depending on the catalyst surface morphology.

Meanwhile, when heat treatment was carried out, the amount of PVP remaining on the catalyst surface decreased. The cell performance was improved by this surface cleaning (i.e. the decomposition of PVP on the catalyst nanoparticles) when the integrated peak area ratio of the CO bridge sites/CO top sites was between 0.5 and 2.0. However, when the ratio was below 0.5 the cell voltage remained low. This may imply that the surface Pt–Pt bonding was not optimized under these conditions.

Fig. 7 shows the relationship between cell performance and integrated peak area ratio of the CO bridge sites/CO top sites. As shown in Fig. 6, this ratio was itself affected by the amount of PVP remaining on the catalyst surface. Therefore, to clarify the specific effect of the ratio, Fig. 7 plots the cell voltage when the amount of PVP on the catalyst surface was fixed at 1.5 wt%.

As can be seen, the cell voltage showed a maximum when the integrated peak area ratio of the CO bridge sites/CO top sites was ca. 1.5. This implies that Pd islands on Pt nanoparticles are highly effective for catalytic activation. According to a DFT calculation, the optimized structure of the Pt/Pd core–shell catalyst featured Pd atoms forming islands on the Pt nanoparticles [20,21].

It is presumed that Pd is relatively easily oxidized by oxygen compared with Pt (i.e. Pd sites are more favorable for the adsorption of oxygen atoms), and the oxygen adsorbed on Pd promotes oxygen adsorption on nearby Pt by electron transfer. Therefore, this implies that the surface Pd atoms improve the catalyst performance.

4. Conclusions

Heat-treated Pt/Pd/C catalysts were characterized by TEM-EDX, SEIRAS, and TG. The optimal Pt/Pd/C catalyst achieved a better performance than Pt/C despite a roughly 50% reduction in the amount of Pt used. Heat treatment of the Pt/Pd/C catalyst effectively improved the cell performance. In core–shell catalysts, the outermost surface has conventionally consisted of Pt. However, the performance can be enhanced if different metals, such as Pd, are used to substitute Pt on the surface, or to form a Pt alloy. On the basis of the present results, the fuel cell performance (oxygen reduction activity) can be improved even if Pd is precipitated in the form of an island without being dissolved as a solid solution.

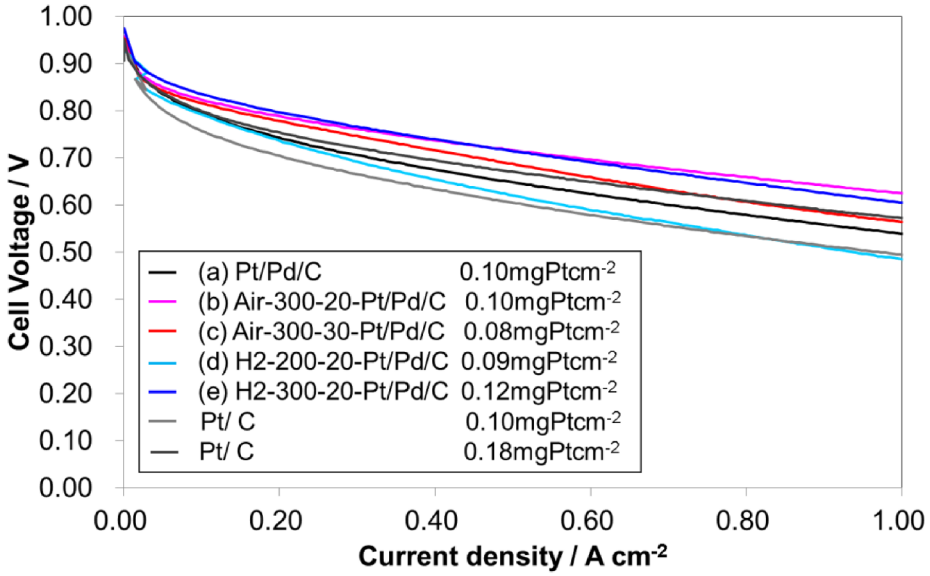

Fig. 5. Cell voltages for (a) Pt/Pd/C, (b) Air-300-20-Pt/Pd/C, (c) Air-300-30-Pt/Pd/C, (d) H2-200-20-Pt/Pd/C, (e) H2-300-20-Pt/Pd/C, and Pt/C. Cell temperature = 80 °C.

Author contribution statements

All authors; Ideas; formulation or evolution of overarching research goals and aims.

K. M., H. N., K. U.; Development or design of methodology; creation of models.

K. M.; M. H.; Verification, whether as a part of the activity or separate, of the overall replication/ reproducibility of results/experiments and other research outputs.

K. M.; Conducting a research and investigation process, specifically performing the experiments.

K. M., H. N.; Preparation, creation and/or presentation of the published work, specifically writing the initial draft (including substantive translation)

T. I., K.U.; Management and coordination responsibility for the research activity planning and execution.

T.I., H. N, K.U.; Acquisition of the financial support for the project leading to this publication.

Declaration of Competing Interest

The authors declare that they have no known competing financial interests or personal relationships that could have appeared to influence the work reported in this paper.

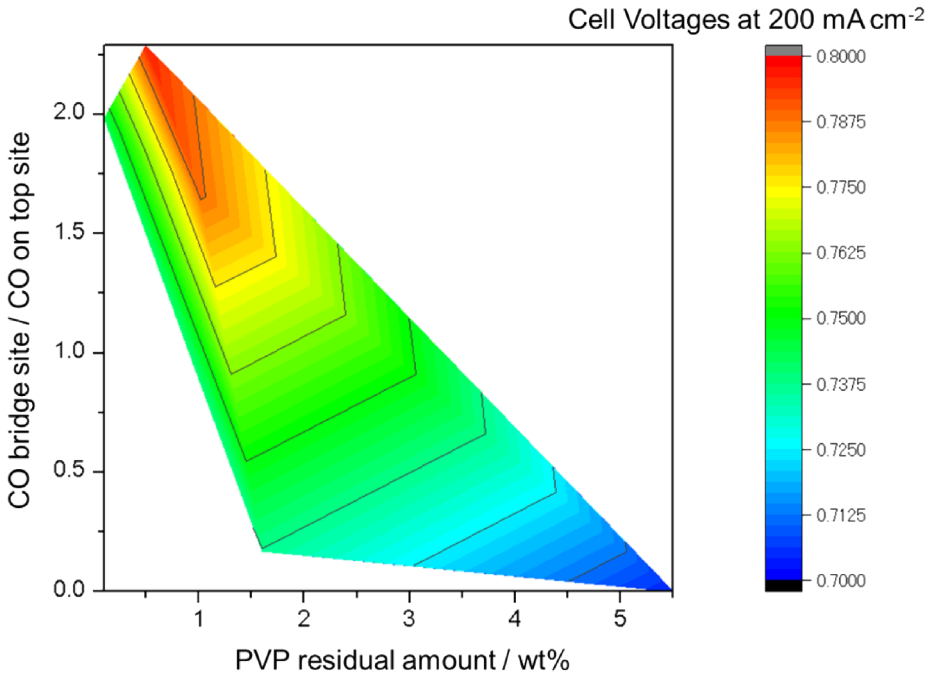

Fig. 6. Contour plot showing the dependence of cell performance on the structural differences of the samples.

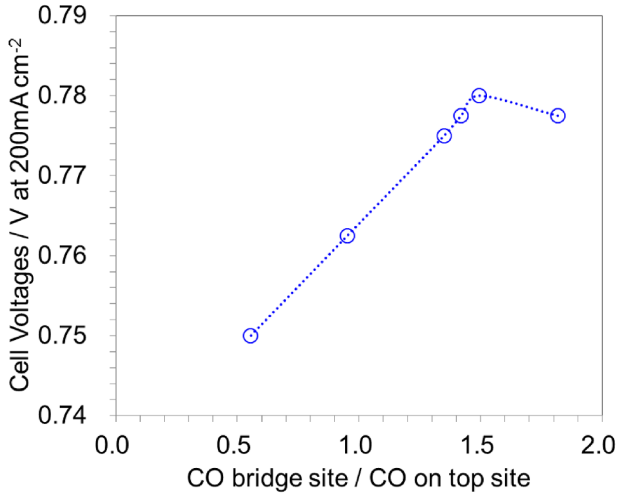

Fig. 7. The relationship between cell performance and ratio of CO bridge sites/CO top sites for a fixed PVP residual amount = 1.5 wt%.

Acknowledgment

This work was supported by the NIMS microstructural characterization platform as a program of "Nanotechnology Platform" of the Ministry of Education, Culture, Sports, Science and Technology (MEXT), Japan.

Appendix A. Supplementary data

Supplementary data to this article can be found online at https://doi.org/10.1016/j.elecom.2020.106736.

References

[1] T. Toda, H. Igarashi, M. Watanabe, J. Electroanal. Chem. 460 (1999) 258–262.
[2] U.A. Paulus, A. Wokaun, G.G. Scherer, T.J. Schmidt, V. Stamenkovic, N.M. Markovic, P.N. Ross, Electrochim. Acta 47 (2002) 3787–3798.
[3] J. Zhang, Y. Mo, M.B. Vukmirovic, R. Klie, K. Sasaki, R.R. Adzic, J. Phy. Chem. B 108 (2004) 10955–10964.
[4] M. Chiwata, H. Yano, S. Ogawa, M. Watanabe, A. Iiyama, H. Uchida, Electrochemistry 84 (2016) 133–137.
[5] L. Wang, W. Gao, Z. Liu, Z. Zeng, Y. Liu, M. Giroux, M. Chi, G. Wang, J. Greeley, X. Pan, C. Wang, ACS Catal. 8 (2018) 35–42.
[6] J. Zhang, M.B. Vukmirovic, Y. Xu, M. Mavrikakis, R.R. Adzic, Angew. Chem. Int. Ed. 44 (2005) 2132–2135.
[7] Y. Wang, N. Toshima, J. Phys. Chem. B 101 (1997) 5301–5306.
[8] H. Naohara, Y. Okamoto, N. Toshima, J. Power Sources 196 (2011) 7510–7513.
[9] Z. Liu, C. Yu, I.A. Rusakova, D. Huang, P. Strasser, Top. Catal. 49 (2008) 241–250.
[10] D. Li, C. Wang, D. Tripkovic, S. Sun, N.M. Markovic, V.R. Stamenkovic, ACS Catal. 2 (2012) 1358–1362.
[11] D. Raciti, J. Kubal, C. Ma, M. Barclay, M. Gonzalez, M. Chi, J. Greeley, K.L. More, C. Wang, Nano Energy 20 (2016) 202–211.
[12] S. Li, D. Umereweneza, Separ. Sci. Tech. 47 (2012) 104–111.
[13] M. Osawa, K. Ataka, K. Yoshii, Y. Nishikawa, Appl. Spectrosc. 47 (1993) 1497–1502.
[14] K. Matsumoto, T. Iijima, M. Hiyoshi, 224th ECS Meeting 1617 Thursday, October 31, 2013.
[15] J.B. Darby, K.M. Myles, Metall. Mater. Trans. 3 (1972) 653–657.
[16] P. Buffat, J. Borel, Phys. Rev. A 13 (1976) 2287–2296.
[17] N. Todoroki, H. Osano, T. Maeyama, H. Yoshida, T. Wadayama, Appl. Surf. Sci. 256 (2009) 943–947.
[18] X. Wang, Y. Orikasa, Y. Takesue, H. Inoue, M. Nakamura, T. Minato, N. Hoshi, Y. Uchimoto, J. Am. Chem. Soc. 135 (2013) 5938–5941.
[19] S. Nagamatsu, S. Takao, G. Samjeské, K. Nagasawa, O. Sekizawa, T. Kaneko, K. Higashi, T. Uruga, S. Gayen, S. Velaga, M.K. Saniyal, Y. Iwasawa, Surf. Sci. 648 (2016) 100–113.
[20] T. Ishimoto, M. Koyama, J. Phys. Chem. Lett. 7 (2016) 736–740.
[21] R. Al-Shareef, M. Harb, Y. Saih, S.O.-Chikh, M.A. Roldan, D.H. Anjum, E. Guyonnet, J.-P. Candy, D.-Y. Jan, S.F. Abdo, A. Aguilar-Tapia, O. Proux, J.-L. Hazemann, J.-M. Basset, J. Catal. 363 (2018) 34–51.